Centrum voor Wiskunde en Informatica
Centre for Mathematics and Computer Science

B. Koren

Multigrid and defect correction
for the steady Navier-Stokes equations

Department of Numerical Mathematics Report NM-R8803 March

The Centre for Mathematics and Computer Science is a research institute of the Stichting Mathematisch Centrum, which was founded on February 11, 1946, as a nonprofit institution aiming at the promotion of mathematics, computer science, and their applications. It is sponsored by the Dutch Government through the Netherlands Organization for the Advancement of Pure Research (Z.W.O.).

Multigrid and Defect Correction for the Steady Navier-Stokes Equations

Barry Koren
Centre for Mathematics and Computer Science
P.O. Box 4079, 1009 AB Amsterdam, The Netherlands

Theoretical and experimental convergence results are presented for multigrid and iterative defect correction applied to finite volume discretizations of the steady, 2D, compressible Navier-Stokes equations. Iterative defect correction is introduced for circumventing the difficulty in finding a solution of discretized equations with a second- or higher-order accurate convective part. As a smoothing technique, use is made of point Gauss-Seidel relaxation with inside the latter, Newton iteration as a basic solution method. The multigrid technique appears to be very efficient for smooth as well as non-smooth problems. Iterative defect correction appears to be very efficient for smooth problems only, though still reasonably efficient for non-smooth problems.

1980 Mathematics Subject Classification: 65B05, 65N10, 65N20, 65N30, 76N10.
Keywords & Phrases: multigrid, defect correction, Navier-Stokes equations.
Note: This work was supported by the European Space Agency (ESA), via Avions Marcel Dassault - Bréguet Aviation (AMD-BA). It has been presented at the Fourth GAMM-Seminar on Robust Multi-Grid Methods, January 22-24, 1988, Kiel.

1. Introduction

1.1. Navier-Stokes equations

The Navier-Stokes equations considered are:

$$\frac{\partial}{\partial x}\begin{bmatrix}\rho u\\ \rho u^2+p\\ \rho uv\\ \rho u(e+\frac{p}{\rho})\end{bmatrix}+\frac{\partial}{\partial y}\begin{bmatrix}\rho v\\ \rho uv\\ \rho v^2+p\\ \rho v(e+\frac{p}{\rho})\end{bmatrix}- \tag{1.1a}$$

$$\frac{1}{Re}\left[\frac{\partial}{\partial x}\begin{bmatrix}0\\ \tau_{xx}\\ \tau_{xy}\\ \tau_{xx}u+\tau_{xy}v+\frac{1}{\gamma-1}\frac{1}{Pr}\frac{\partial(c^2)}{\partial x}\end{bmatrix}+\frac{\partial}{\partial y}\begin{bmatrix}0\\ \tau_{xy}\\ \tau_{yy}\\ \tau_{yy}v+\tau_{xy}u+\frac{1}{\gamma-1}\frac{1}{Pr}\frac{\partial(c^2)}{\partial y}\end{bmatrix}\right]=0,$$

with

$$\begin{aligned}\tau_{xx}&=\frac{4}{3}\frac{\partial u}{\partial x}-\frac{2}{3}\frac{\partial v}{\partial y},\\ \tau_{xy}&=\frac{\partial u}{\partial y}+\frac{\partial v}{\partial x},\\ \tau_{yy}&=\frac{4}{3}\frac{\partial v}{\partial y}-\frac{2}{3}\frac{\partial u}{\partial x}.\end{aligned} \tag{1.1b}$$

For a detailed description of the various quantities used, assumptions made and so on, we refer to any standard textbook. Suffice to say here that these are the full Navier-Stokes equations with as main assumptions made: zero bulk viscosity and constant diffusion coefficients. (So, the flow is assumed to be laminar and its diffusion coefficients are assumed to be temperature independent.)

1.2. Discretization method

For a detailed description of the discretization method, we refer to [8,9]. Here, a brief summary is given of its main characteristics only.

Since we also want to be able to compute Euler flow solutions (with possibly occurring discontinuities), the Navier-Stokes equations (1.1) are discretized in integral form. A straightforward and simple discretization of the integral form is obtained by subdividing the integration region into finite volumes, and by requiring that the integral form holds for each finite volume separately. This discretization requires an evaluation of a convective and diffusive flux vector at each volume wall.

1.2.1. Evaluation of convective fluxes. Based on experience with the Euler equations [3,4,5,6,7,11], for the evaluation of the convective fluxes we prefer an upwind approach. In here, the convective flux vector is assumed to be constant along each volume wall, and to be determined by a uniformly constant left and right state only. For the 1D Riemann problem thus obtained, an approximate Riemann solver is applied.

The choice of the left and right state, to be used as entries for the approximate Riemann solver, determines the accuracy of the convective discretization. First-order accuracy is simply obtained by taking the left and right state equal to that in the corresponding adjacent volume [5]. Higher-order accuracy is obtained by applying low-degree piecewise polynomial functions, using two or three adjacent volume states for the left and right state separately [3]. The higher-order accurate polynomial function used is van Leer's κ-function [13]. This function is general in the sense that it contains a variable $\kappa \in [-1,1]$ that can be used for chosing any higher-order approximation ranging from central ($\kappa = 1$) to fully one-sided upwind ($\kappa = -1$). A survey of some characteristic κ-values and their corresponding properties in the case of Euler flow computations has been given in [7]. As an optimal value for κ in the case of Navier-Stokes flows, we found by error analysis: $\kappa = 1/3$ [10]. For this specific κ-value, we also constructed a new (monotonicity preserving) limiter [10].

For the approximate Riemann solver, we considered two possibilities which both have continuous differentiability (a prerequisite for applying Newton's method), namely OSHER'S [14] and van LEER'S [12] scheme. Theoretical analysis has shown that Osher's scheme is to be preferred above van Leer's scheme [10]. This has been confirmed by computations [10].

1.2.2. Evaluation of diffusive fluxes. For the evaluation of the diffusive fluxes, use is made of the standard central technique as outlined in [15]. For the necessary computation at each volume wall of $\nabla u, \nabla v$ and ∇c^2, the technique uses (at inner volume walls) a shifted volume overlying the volume wall considered.

2. CONVERGENCE OF MULTIGRID

The same multigrid method which has been used with success for the first-order discretized Euler equations [5] is taken as a point of departure for both the first- and second-order discretized Navier-Stokes equations. The method makes use of symmetric point Gauss-Seidel relaxation as a smoothing technique. In here, one or more Newton steps are performed for the collective relaxation of the four state vector components in each finite volume. (Usually, the tolerance for the Newton iteration is so large that in a substantial majority of all cells, only one Newton step is performed.) For the first-order discretized Euler equations, point Gauss-Seidel relaxation turned out to be a good smoother, thus enabling a good multigrid acceleration. However, for higher-order discretized Euler equations the good smoothing property is lost. Obviously, this will also be the case for Navier-Stokes flows with high Reynolds number. We do not anticipate to this by looking for some remedy already, but we investigate at first how smoothing evolves with increasingly dominating convection. The complete multigrid method as developed for Euler (see [11] for a detailed description) is carried over to Navier-Stokes, with as the only a priori change, a replacement of the piecewise constant correction prolongation by a bilinear prolongation [8], thus satisfying the rule that the sum of orders of the prolongation and restriction should exceed the order of the differential equation ($m_p + m_r > 2m$) [1]. Notice that as a consequence the Galerkin property [5] is definitely lost.

2.1. Investigation method

Both theoretical and experimental convergence results are presented; the theoretical results being obtained by local mode analysis, the experimental results being obtained by considering two standard flow problems; a smooth and a non-smooth problem.

2.1.1. Smoothing analysis. For the smoothing analysis we consider the linear and scalar convection diffusion equation

$$\frac{\partial u}{\partial x} + \frac{\partial u}{\partial y} - \epsilon\left(\frac{\partial^2 u}{\partial x^2} + \frac{\partial^2 u}{\partial x \partial y} + \frac{\partial^2 u}{\partial y^2}\right) = 0. \tag{2.1}$$

For the integral form to be considered for each finite volume $\Omega_{j,k}, j=1,2,...,J,\ k=1,2,...,K$, we take:

$$\oint_{\partial\Omega_{j,k}} (un_x + un_y)ds - \epsilon \oint_{\partial\Omega_{j,k}} \left(\frac{\partial u}{\partial x}n_x + \frac{\partial u}{\partial x}n_y + \frac{\partial u}{\partial y}n_y\right)ds = 0,\ \forall_{j,k}, \tag{2.2}$$

with $\partial\Omega_{j,k}$ the boundary of $\Omega_{j,k}$. The two parts of the discretization to be modelled are (i) an upwind treatment of convection, either first- or higher-order accurate (non-limited $\kappa = 1/3$), and (ii) a central second-order accurate treatment of diffusion. Assuming a finite volume grid with equidistant walls parallel to the x- and y-axis ($\Delta x = \Delta y = h$, fig. 2.1), the evaluation of convective flux terms yields:

$$\begin{aligned} \oint_{\partial\Omega_{j,k}} un_x ds &= (u^l_{j+\frac{1}{2},k} - u^l_{j-\frac{1}{2},k})h, \\ \oint_{\partial\Omega_{j,k}} un_y ds &= (u^l_{j,k+\frac{1}{2}} - u^l_{j,k-\frac{1}{2}})h, \end{aligned} \tag{2.3a}$$

with

$$\begin{aligned} u^l_{j+\frac{1}{2},k} &= \alpha_1 u_{j-1,k} + \alpha_2 u_{j,k} + \alpha_3 u_{j+1,k}, \\ u^l_{j,k+\frac{1}{2}} &= \alpha_1 u_{j,k-1} + \alpha_2 u_{j,k} + \alpha_3 u_{j,k+1}, \end{aligned} \tag{2.3b}$$

and similar expressions for $u^l_{j-\frac{1}{2},k}$ and $u^l_{j,k-\frac{1}{2}}$ (the coefficients α_i still free).

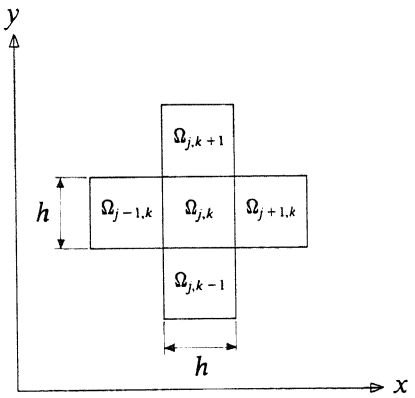

Fig. 2.1. Model volume $\Omega_{j,k}$ with neighbours

For the diffusive terms we get:

$$\begin{aligned} \oint_{\partial\Omega_{j,k}} \frac{\partial u}{\partial x}n_x ds &= \{(\frac{\partial u}{\partial x})_{j+\frac{1}{2},k} - (\frac{\partial u}{\partial x})_{j-\frac{1}{2},k}\}h, \\ \oint_{\partial\Omega_{j,k}} \frac{\partial u}{\partial x}n_y ds &= \{(\frac{\partial u}{\partial x})_{j,k+\frac{1}{2}} - (\frac{\partial u}{\partial x})_{j,k-\frac{1}{2}}\}h, \\ \oint_{\partial\Omega_{j,k}} \frac{\partial u}{\partial y}n_y ds &= \{(\frac{\partial u}{\partial y})_{j,k+\frac{1}{2}} - (\frac{\partial u}{\partial y})_{j,k-\frac{1}{2}}\}h, \end{aligned} \tag{2.4a}$$

with

$$\begin{aligned} (\frac{\partial u}{\partial x})_{j+\frac{1}{2},k} &= \frac{1}{h^2}\oint_{\partial\Omega_{j+\frac{1}{2},k}} un_x ds = \frac{1}{h}(u_{j+1,k} - u_{j,k}), \\ (\frac{\partial u}{\partial x})_{j,k+\frac{1}{2}} &= \frac{1}{h^2}\oint_{\partial\Omega_{j,k+\frac{1}{2}}} un_x ds = \frac{1}{h}\{\frac{1}{4}(u_{j,k} + u_{j+1,k} + u_{j,k+1} + u_{j+1,k+1}) - \\ &\qquad \frac{1}{4}(u_{j-1,k} + u_{j,k} + u_{j-1,k+1} + u_{j,k+1})\} = \\ &= \frac{1}{4h}(u_{j+1,k} + u_{j+1,k+1} - u_{j-1,k} - u_{j-1,k+1}), \\ (\frac{\partial u}{\partial y})_{j,k+\frac{1}{2}} &= \frac{1}{h^2}\oint_{\partial\Omega_{j,k+\frac{1}{2}}} un_y ds = \frac{1}{h}(u_{j,k+1} - u_{j,k}), \end{aligned} \tag{2.4b}$$

and similar expressions for $(\frac{\partial u}{\partial x})_{j-\frac{1}{2},k}$, $(\frac{\partial u}{\partial x})_{j,k-\frac{1}{2}}$ and $(\frac{\partial u}{\partial y})_{j,k-\frac{1}{2}}$. In (2.4b), $\partial\Omega_{j+\frac{1}{2},k}$ and $\partial\Omega_{j,k+\frac{1}{2}}$ denote the boundary of shifted volume $\Omega_{j+\frac{1}{2},k}$ respectively $\Omega_{j,k+\frac{1}{2}}$ (fig. 2.2).

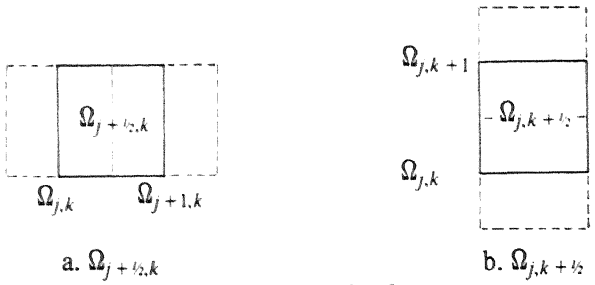

a. $\Omega_{j+\frac{1}{2},k}$ b. $\Omega_{j,k+\frac{1}{2}}$

Fig. 2.2. Shifted volumes

With the previous flux evaluations we get for each finite volume $\Omega_{j,k}$ the algebraic equation:

$$\begin{aligned}
&\tfrac{1}{4}\tfrac{\epsilon}{h}u_{j-1,k+1}+(\alpha_3-\tfrac{\epsilon}{h})u_{j,k+1}-\tfrac{1}{4}\tfrac{\epsilon}{h}u_{j+1,k+1}-\\
&\alpha_1 u_{j-2,k}+(\alpha_1-\alpha_2-\tfrac{\epsilon}{h})u_{j-1,k}+(2\alpha_2-2\alpha_3+4\tfrac{\epsilon}{h})u_{j,k}+(\alpha_3-\tfrac{\epsilon}{h})u_{j+1,k}-\\
&\tfrac{1}{4}\tfrac{\epsilon}{h}u_{j-1,k-1}+(\alpha_1-\alpha_2-\tfrac{\epsilon}{h})u_{j,k-1}+\tfrac{1}{4}\tfrac{\epsilon}{h}u_{j+1,k-1}-\\
&\alpha_1 u_{j,k-2}=0,
\end{aligned} \tag{2.5}$$

with corresponding stencil:

$k+1$		$\frac{1}{4}\frac{\epsilon}{h}$	$\alpha_3-\frac{\epsilon}{h}$	$-\frac{1}{4}\frac{\epsilon}{h}$
k	$-\alpha_1$	$\alpha_1-\alpha_2-\frac{\epsilon}{h}$	$2\alpha_2-2\alpha_3+4\frac{\epsilon}{h}$	$\alpha_3-\frac{\epsilon}{h}$
$k-1$		$-\frac{1}{4}\frac{\epsilon}{h}$	$\alpha_1-\alpha_2-\frac{\epsilon}{h}$	$\frac{1}{4}\frac{\epsilon}{h}$
$k-2$			$-\alpha_1$	
	$j-2$	$j-1$	j	$j+1$

(2.6)

The parameter ϵ/h in (2.5) and (2.6) models the inverse of the mesh Reynolds number. Of course, for the model grid considered, the finite volume discretization boils down to a finite difference discretization for which the above stencil can be given directly. The purpose of the previous finite volume derivation merely is to illustrate for a model problem, the way of evaluating the intricate convective and diffusive fluxes arising for (1.1).

For point Gauss-Seidel relaxation applied to (2.5), four basically different sweep directions can be considered: downwind, upwind and twice crosswind. Introducing the counter n for the number of sweeps performed, these four possibilities can be illustrated as has been done in fig. 2.3. (In fig. 2.3, $u_{j,k}^{n+1}$ denotes the $(n+1)$th iterand of $u_{j,k}$.)

$k+1$	u^n	u^n	u^n
k	u^{n+1}	u^{n+1}	u^n
$k-1$	u^{n+1}	u^{n+1}	u^{n+1}
	$j-1$	j	$j+1$

a. Downwind

$k+1$	u^{n+1}	u^{n+1}	u^{n+1}
k	u^n	u^{n+1}	u^{n+1}
$k-1$	u^n	u^n	u^n
	$j-1$	j	$j+1$

b. Upwind

$k+1$	u^n	u^n	u^n
k	u^n	u^{n+1}	u^{n+1}
$k-1$	u^{n+1}	u^{n+1}	u^{n+1}
	$j-1$	j	$j+1$

c. Crosswind

$k+1$	u^{n+1}	u^{n+1}	u^{n+1}
k	u^{n+1}	u^{n+1}	u^n
$k-1$	u^n	u^n	u^n
	$j-1$	j	$j+1$

d. Crosswind

Fig. 2.3. Basic sweep directions, convection direction:

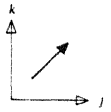

For local mode analysis, we introduce in the standard way: (i) the iteration error

$$\delta_{j,k}^{n} = u_{j,k}^{*} - u_{j,k}^{n}, \tag{2.7}$$

with $u_{j,k}^{*}$ the converged numerical solution in $\Omega_{j,k}$, and: (ii) the Fourier form

$$\delta_{j,k}^{n} = D\mu^{n} e^{i(\omega_1 j + \omega_2 k)h}, \tag{2.8}$$

with D some constant, μ the amplification factor, and ω_1 and ω_2 the error frequency in j- respectively k-direction. The frequencies to be considered are: $\pi/2h \leqslant |\omega_1|, |\omega_2| \leqslant \pi/h$. By introducing (2.8) into (2.5), defining $\theta_1 = \omega_1 h, \theta_2 = \omega_2 h$, and considering for instance the downwind relaxation sweep, we get:

$e^{i\theta_2}$		$\frac{1}{4}\frac{\epsilon}{h}$	$\alpha_3 - \frac{\epsilon}{h}$	$-\frac{1}{4}\frac{\epsilon}{h}$
1	$-\alpha_1\mu$	$(\alpha_1 - \alpha_2 - \frac{\epsilon}{h})\mu$	$(2\alpha_2 - 2\alpha_3 + 4\frac{\epsilon}{h})\mu$	$\alpha_3 - \frac{\epsilon}{h}$
$e^{-i\theta_2}$		$-\frac{1}{4}\frac{\epsilon}{h}\mu$	$(\alpha_1 - \alpha_2 - \frac{\epsilon}{h})\mu$	$\frac{1}{4}\frac{\epsilon}{h}\mu$
$e^{-2i\theta_2}$			$-\alpha_1\mu$	
	$e^{-2i\theta_1}$	$e^{-i\theta_1}$	1	$e^{i\theta_1}$

(2.9)

with $\pi/2 \leqslant |\theta_1|, |\theta_2| \leqslant \pi$.

Results for this smoothing analysis are given in section 2.2.

2.1.2. Experiments. The smooth flow problem considered is a subsonic flat plate flow at $Re = 100$, for which we can use the Blasius solution [16] as a reference solution. The non-smooth problem considered is a supersonic flat plate flow at $Re = 2.96\ 10^5$, with an oblique shock wave impinging upon the flat plate boundary layer. This problem has been taken from [2]. For both flow problems, use is made of: $\gamma = 1.4$ and $Pr = 0.71$.

Geometry and boundary conditions as applied for the subsonic flat plate flow are given in fig. 2.4. As far as convection is concerned, the eastern boundary is considered to be an outflow boundary. For diffusion, the northern, southern and eastern boundary are assumed to be far-field boundaries with zero diffusion. For this subsonic problem we only apply grids composed of square finite volumes. The coarsest grid in all multigrid computations is the 4×2-grid given in fig. 2.4. For details about boundary conditions and so on, we refer to [8].

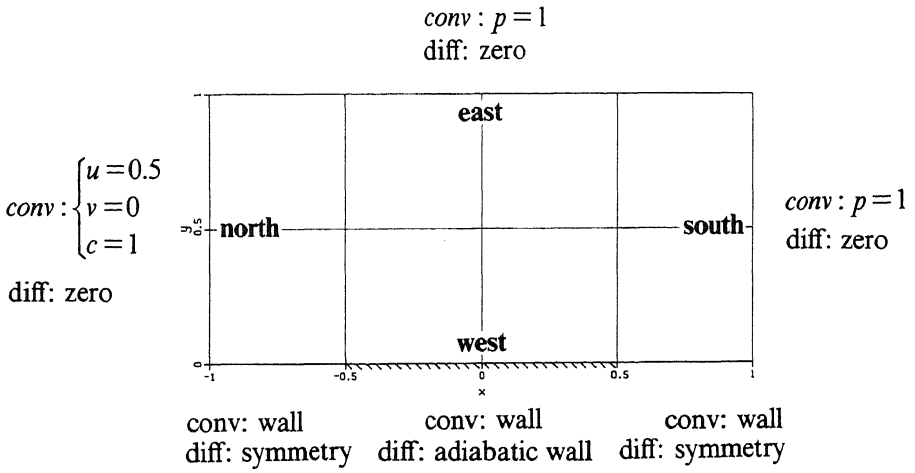

Fig. 2.4. Geometry, boundary conditions and coarsest grid subsonic flat plate flow (conv: convection, diff: diffusion)

Geometry and boundary conditions for the supersonic flat plate flow are indicated globally in fig. 2.5. For details see again [8]. In all multigrid computations, the coarsest grid applied is the 5×2-grid given in fig. 2.5. The grid has been optimized for convection by introducing a stretching in j-direction, and in particular by aligning it with the impinging shock wave [9]. A grid adaptation for diffusion has been realized by introducing stretching in k-direction only. Notice that this problem essentially differs from the previous problem, both in flow and in grid.

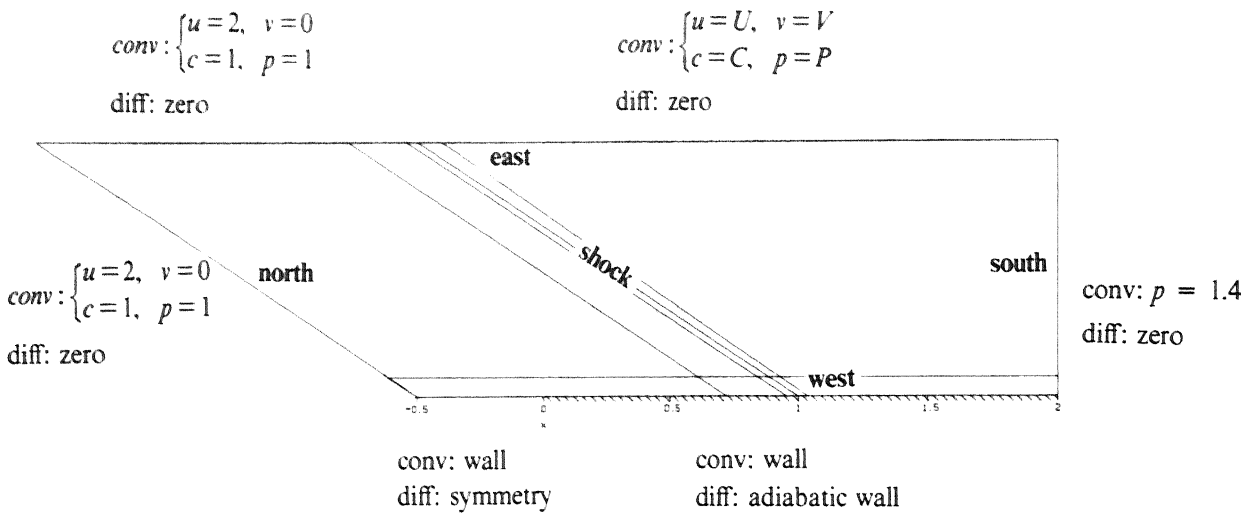

Fig. 2.5. Geometry, boundary conditions and coarsest grid supersonic flat plate flow (conv: convection, diff: diffusion)

2.2. Results

2.2.1. First-order discretized equations. For the first-order accurate model discretization we have $\alpha_1 = \alpha_3 = 0, \alpha_2 = 1$. With this the general 11-point stencil (2.6) reduces to the following 9-point stencil

$k+1$	$\frac{1}{4}\frac{\epsilon}{h}$	$-\frac{\epsilon}{h}$	$-\frac{1}{4}\frac{\epsilon}{h}$
k	$-(1+\frac{\epsilon}{h})$	$2+4\frac{\epsilon}{h}$	$-\frac{\epsilon}{h}$
$k-1$	$-\frac{1}{4}\frac{\epsilon}{h}$	$-(1+\frac{\epsilon}{h})$	$\frac{1}{4}\frac{\epsilon}{h}$
	$j-1$	j	$j+1$

(2.10)

Introducing the iteration error in the way suggested before we get the smoothing results given in fig. 2.6. In fig. 2.6a, for each of the four possible sweep directions, the smoothing factor $\mu_s = \sup|\mu(\theta_1, \theta_2)|$, $\pi/2 \leqslant |\theta_1|, |\theta_2| \leqslant \pi$ is given as a function of ϵ/h. In fig. 2.6b, for $\epsilon/h = 1$, the corresponding distributions $|\mu(\theta_1, \theta_2)|$, $\pi/2 \leqslant |\theta_1|, |\theta_2| \leqslant \pi$ are given. (All four distributions are point-symmetric with respect to $\theta_1 = 0, \theta_2 = 0$.) Clearly visible in fig. 2.6a is the good smoothing for any value of ϵ/h and any convection direction, when sweeping alternatingly in all four different directions (for instance by applying symmetric sweeps and by using a different diagonal sweep direction in pre- and post-relaxation). Robustness and efficiency seem to be ready to hand.

For the subsonic flat plate flow, the multigrid method's behaviour is illustrated in fig. 2.7a. The measure of grid independence is illustrated by convergence histories obtained on a 16×8-, a 32×16- and a 64×32-grid. For the flow considered, the method appears to be nearly grid independent. In the same figure, the multigrid effectiveness is illustrated by giving the convergence history for a single grid computation on the 64×32-grid. Further, in the same figure, the influence of the higher-order accuracy of the prolongation is illustrated by giving also the convergence history for a strategy with $m_p = 1$ (so violating the rule $m_p + m_r > 2m$ [1]). In agreement with [18], for this convection dominated flow, the positive influence of the second-order prolongation already appears to be negligible. Using the Blasius solution as a reference, in [8] it is shown that only a single FAS-cycle is sufficient for converging to discretization error accuracy.

For the supersonic flat plate flow, results are shown in fig. 2.7b for a 20×8-, a 40×16- and a 80×32-grid. Here we used the first-order prolongation only. Despite of the slight deterioration with respect to the subsonic flow, the multigrid properties are still acceptable.

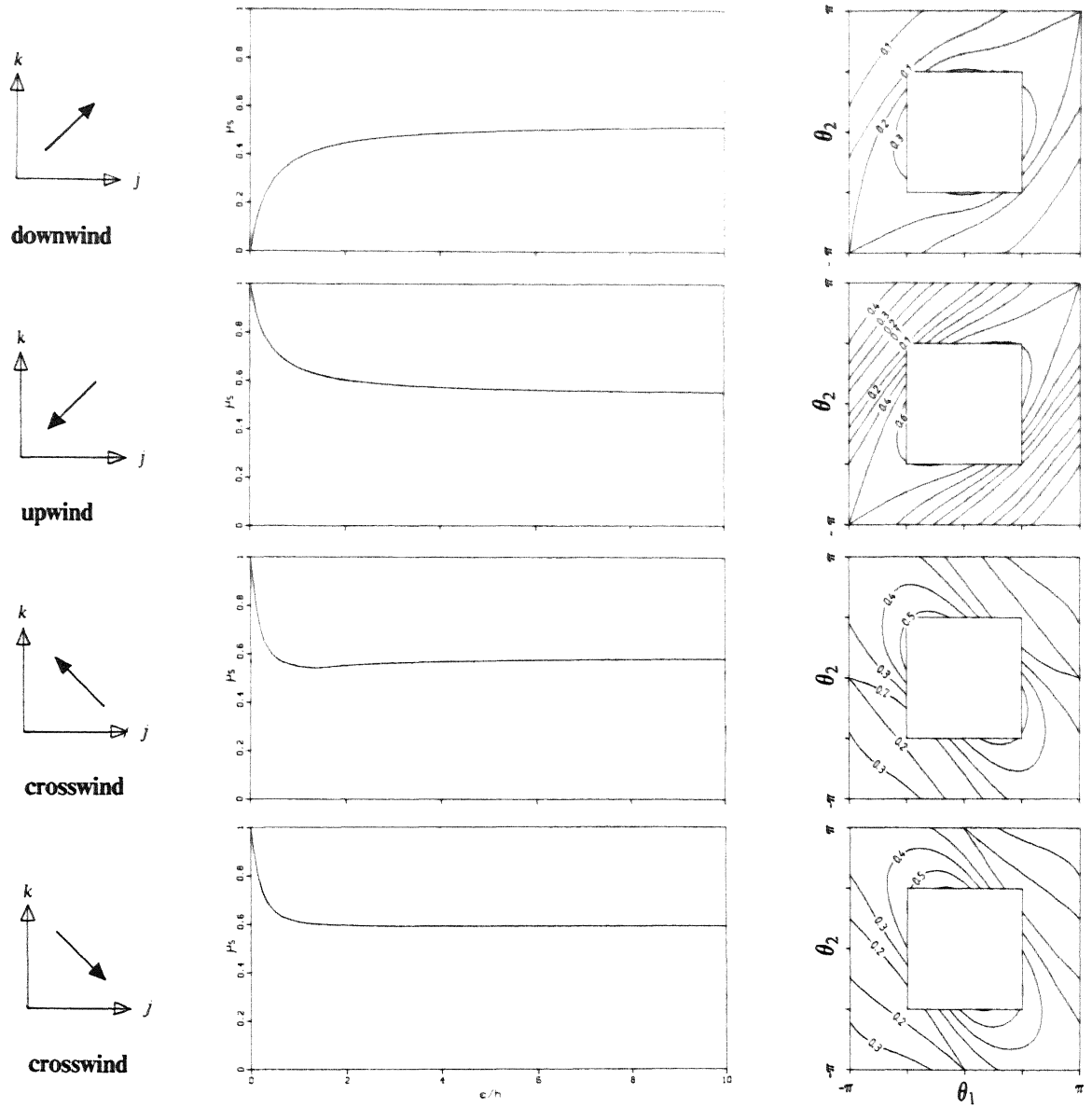

a. Versus ϵ/h b. For $\epsilon/h=1$

Fig. 2.6. Smoothing factors point Gauss-Seidel relaxation, first-order discretized model equation

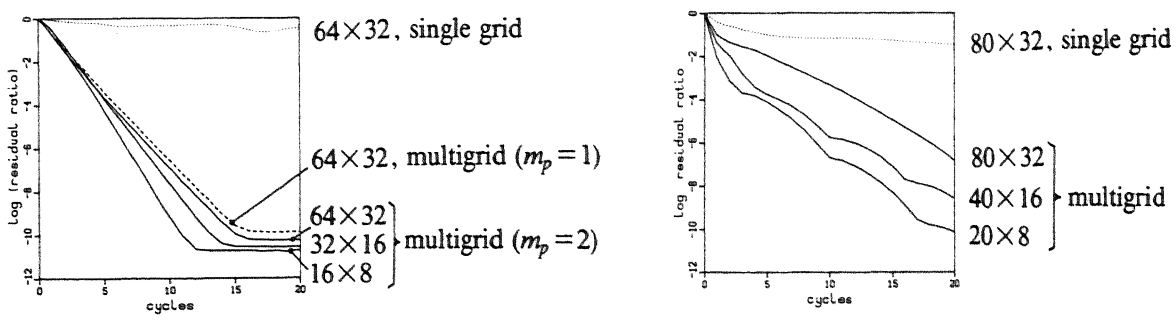

a. Subsonic flat plate flow b. Supersonic flat plate flow

Fig. 2.7. Multigrid behaviour first-order discretized Navier-Stokes equations

2.2.2. Second-order discretized equations. For the second-order accurate model discretization we have: $\alpha_1 = -1/6, \alpha_2 = 5/6, \alpha_3 = 1/3$ [9]. With these values, (2.6) becomes

	$j-2$	$j-1$	j	$j+1$
$k+1$		$\frac{1}{4}\frac{\epsilon}{h}$	$\frac{1}{3}-\frac{\epsilon}{h}$	$-\frac{1}{4}\frac{\epsilon}{h}$
k	$\frac{1}{6}$	$-(1+\frac{\epsilon}{h})$	$1+4\frac{\epsilon}{h}$	$\frac{1}{3}-\frac{\epsilon}{h}$
$k-1$		$-\frac{1}{4}\frac{\epsilon}{h}$	$-(1+\frac{\epsilon}{h})$	$\frac{1}{4}\frac{\epsilon}{h}$
$k-2$			$\frac{1}{6}$	

(2.11)

For the four basic sweep directions, this yields the smoothing results given in fig. 2.8. Only for $\epsilon/h > 1$ there is some valuable smoothing. For problems which are locally convection dominated, say with $\epsilon/h \ll 1$ locally, the present smoothing factors are unacceptable, except perhaps for those belonging to the purely downwind sweep. Since purely downwind relaxation sweeps are not feasible in practice, and since no specific alternation of sweep directions suffices, another remedy has to be found. Inspired by its rather successful application in the Euler flow method [3,7], iterative defect correction is considered for this purpose.

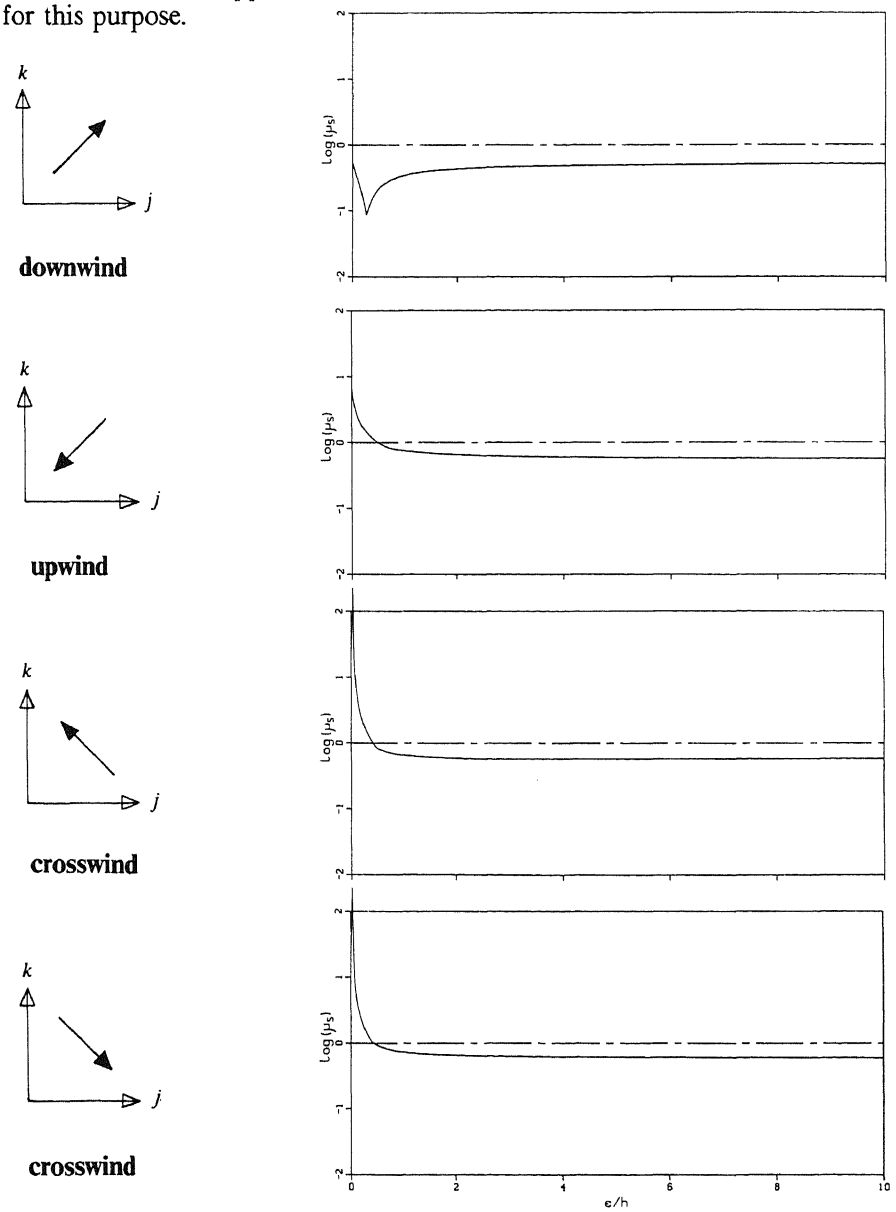

Fig. 2.8. Smoothing factors point Gauss-Seidel relaxation, second-order discretized model equation

3. Convergence of iterative defect correction

The iterative defect correction (IDeC-) method can be written as:

$$\begin{aligned} &\tilde{F}_h(q_h^1) = 0, \\ &\tilde{F}_h(q_h^{n+1}) = \tilde{F}_h(q_h^n) - \omega F_h(q_h^n), \quad n = 1,2,...,N. \end{aligned} \tag{3.1}$$

with the superscript n denoting the iteration counter and ω a possible damping factor. (A standard value for ω is $\omega = 1$.) The two discrete operators considered are: the higher-order accurate operator F_h which for the model problem is defined by (2.11), and: the approximate operator $\tilde{F}_h$, the operator to be inverted. A requirement to be fulfilled by $\tilde{F}_h$ as seen in section 2.2.2, is that it must have a first-order accurate convective part only. The choice of the diffusive part is still free. Two in this sense extreme possibilities are already available: (i) the operator without diffusive terms as used in the Euler work, and (ii) the operator with second-order accurate diffusion as just considered in section 2.2.1. The advantage of the first approximate operator is its greater simplicity. For the second operator this is its closer resemblance to the target operator F_h. It complies with the theory that for sufficiently smooth problems, the solution will be second-order accurate after a single IDeC-cycle only [1]. As an intermediate alternative we also consider the approximate operator which neglects the cross derivatives. This operator will combine, in some sense, simplicity and good resemblance.

As in section 2, both theoretical and experimental results are presented. The theoretical results are obtained by local mode analysis for the same model problem as in section 2, and the experimental results are obtained by considering the same two flow problems as in section 2. Local mode analysis is made for both the outer and inner iteration (convergence respectively smoothing analysis).

3.1. Theoretical results

Concisely written, the three approximate operators to be considered are: (i) the first-order accurate convection operator

$$\begin{array}{c|cc} k & -1 & 2 \\ k-1 & & -1 \\ \hline & j-1 & j \end{array} \tag{3.2}$$

(ii) the zeroth-order accurate convection-diffusion operator

$$\begin{array}{c|ccc} k+1 & & -\frac{\epsilon}{h} & \\ k & -(1+\frac{\epsilon}{h}) & 2+4\frac{\epsilon}{h} & -\frac{\epsilon}{h} \\ k-1 & & -(1+\frac{\epsilon}{h}) & \\ \hline & j-1 & j & j+1 \end{array} \tag{3.3}$$

and, (iii) the first-order accurate convection-diffusion operator (2.10).

For the linear model problem (2.1), iteration (3.1) can be rewritten as

$$\begin{aligned} &\tilde{F}_h(u_h^1) = 0, \\ &\tilde{F}_h(u_h^{n+1}) = (\tilde{F}_h - \omega F_h)(u_h^n), \quad n = 1,2,...,N. \end{aligned} \tag{3.4}$$

Introducing as before the iteration error (2.7) in its Fourier form (2.8), we can write for the convergence factor μ:

$$\mu(\theta_1,\theta_2) = 1 - \omega F_h(\theta_1,\theta_2)\tilde{F}_h^{-1}(\theta_1,\theta_2), \; 0 \leqslant |\theta_1|,|\theta_2| \leqslant \pi. \tag{3.5}$$

For $\omega = 1$, convergence results are given in fig. 3.1. In fig. 3.1a, for each of the three approximate operators (3.2), (3.3) and (2.10), the convergence factor $\mu_c = \sup|\mu(\theta_1,\theta_2)|$, $\omega = 1$, $0 \leqslant |\theta_1|,|\theta_2| \leqslant \pi$ is given as a function of ϵ/h. In fig. 3.1b, for $\epsilon/h = 4/9$, $\epsilon/h = 1$ and $\epsilon/h = \infty$, the corresponding distributions of $|\mu(\theta_1,\theta_2)|$, $\omega = 1$, $0 \leqslant |\theta_1|$, $|\theta_2| \leqslant \pi$ are given. (Again, all distributions are point-symmetric with respect to $\theta_1 = 0$, $\theta_2 = 0$.) From fig. 3.1a it appears that for small values of ϵ/h, the approximate operator (3.2) yields the best convergence rate. However, as was to be expected, its convergence starts to deteriorate (from $\epsilon/h = 4/9$) and finally turns into divergence. Even for high-Reynolds number flows, local regions with diffusion dominating convection may arise. Therefore, approximate operator (3.2) has to be rejected. As far as the convergence rate of the two remaining operators is concerned, the 9-point operator (2.10) clearly is to be preferred above the 5-point alternative (3.3).

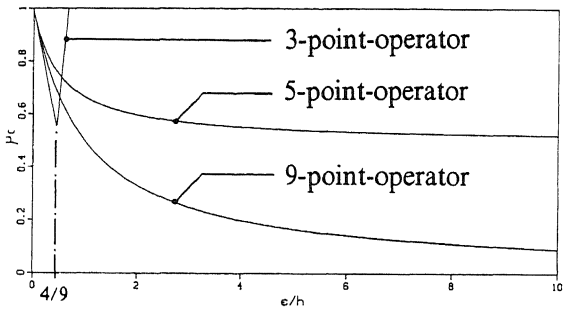

a. Versus ϵ/h

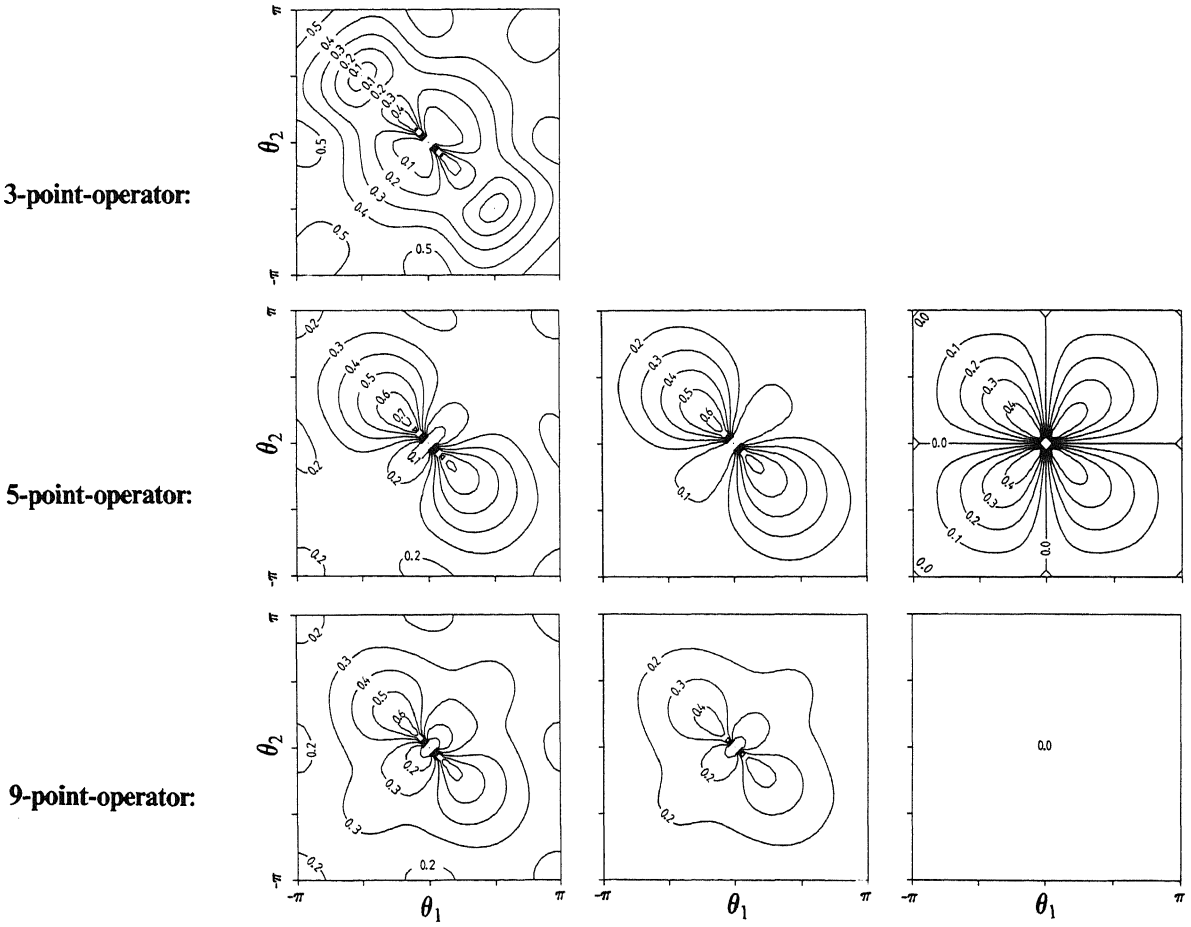

b. For $\epsilon/h=4/9$, $\epsilon/h=1$ and $\epsilon/h=\infty$

Fig. 3.1. Convergence factors iterative defect correction, second-order discretized model equation

However, the 5-pointer might behave better in the inner iteration (Gauss-Seidel accelerated by multigrid). In fig. 3.2, for the four basic sweep directions, its smoothing factors μ_s are given as a function of ϵ/h. The smoothing factors which were already presented for the 9-point operator (fig. 2.6) have been added. It appears that both operators practically have the same good smoothing behaviour, the 5-pointer being only slightly better. Because of its superior behaviour in IDeC, we prefer the 9-pointer as operator to be inverted. (Its relative complexity is taken for granted.)

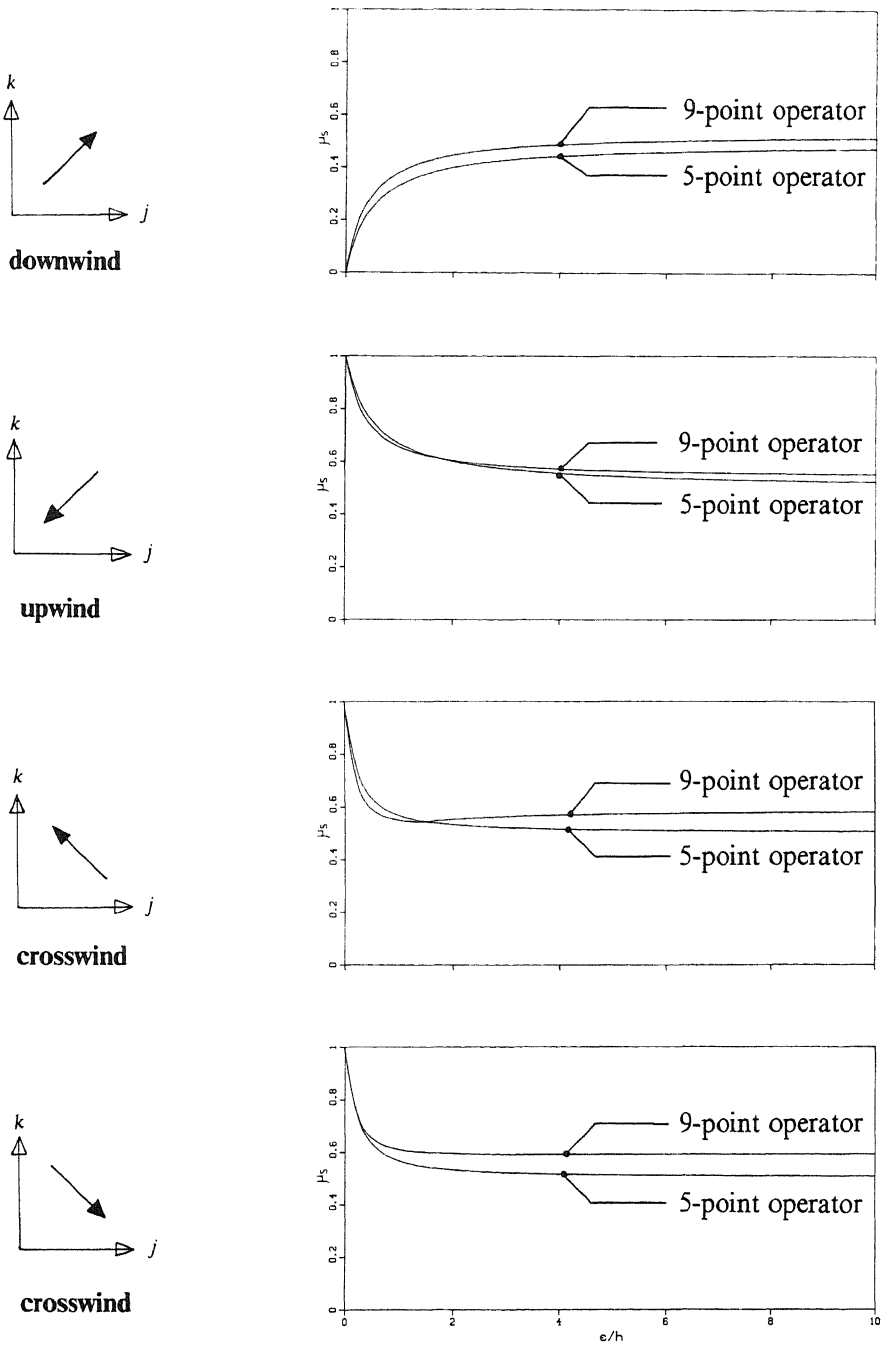

Fig. 3.2. Smoothing factors point Gauss-Seidel relaxation, zeroth- and first-order discretized model equation

3.2. Experimental results

For the subsonic flat plate flow, results are shown in fig. 3.3. Given for the 16×8-, 32×16- and 64×32-grid is the velocity profile obtained on the middle of the plate after 1 and 50 IDeC-cycles. (In all cases we performed a single FAS-cycle per IDeC-cycle only.) In agreement with theory [1], only a single IDeC-cycle appears to be sufficient for obtaining higher-order accuracy.

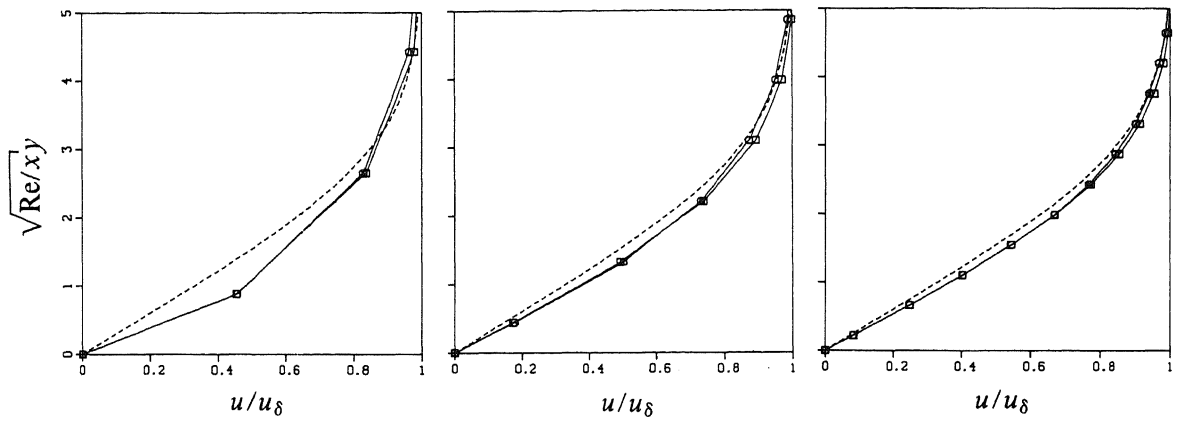

a. On 16 × 8-grid b. On 32 × 16-grid c. On 64 × 32-grid

Fig. 3.3. Velocity profiles subsonic flat plate flow, $Re = 100$, $x = 0.5$ (○: after 1 IDeC-cycle, □ : after 50 IDeC-cycles, ------: Blasius solution)

For the supersonic flat plate flow, the second-order accurate results are given in fig. 3.4. Here, we had to use the limiter, and further we had to take $\omega = ½$. Compared with the subsonic flat plate flow, again a decrease in convergence rate is observed.

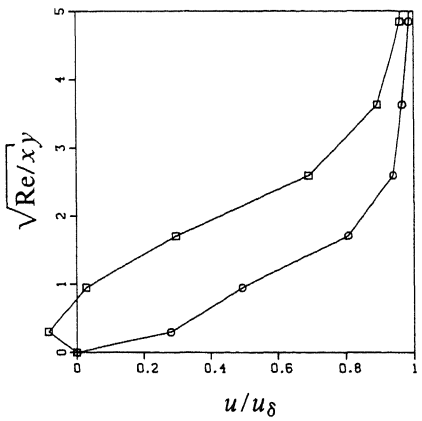

Fig. 3.4. Velocity profiles supersonic flat plate flow, $Re = 2.96\ 10^5$, $x = 1$ (○: after 1 IDeC-cycle, □ : after 50 IDeC-cycles)

4. Conclusions

For the first-order discretized Navier-Stokes equations, point Gauss-Seidel relaxation accelerated by multigrid has been applied to the target equations directly. Both theory and practice show a fast convergence for smooth problems. For problems with non-smooth solutions and (consequently) non-uniform grids, practical computations show the same.

For the second-order discretized equations, iterative defect correction has been introduced, with point Gauss-Seidel and multigrid applied to the first-order discretized equations as an approximate solver. Both theory and practice show a fast convergence for smooth problems. For problems with non-smooth solutions and non-uniform grids the convergence rate is less good, though still satisfactory.

Acknowledgement

The author wants to thank dr. Hemker and prof. Wesseling for their constructive comments.

References

1. W. Hackbusch (1985). *Multigrid Methods and Applications.* Springer, Berlin.
2. R.J. Hakkinen, I. Greber, L. Trilling and S.S. Abarbanel (1958). *The Interaction of an Oblique Shock Wave with a Laminar Boundary Layer.* NASA-memorandum 2-18-59 W.
3. P.W. Hemker (1986). *Defect Correction and Higher Order Schemes for the Multi Grid Solution of the Steady Euler Equations.* Proceedings of the 2nd European Conference on Multigrid Methods, Cologne 1985, Springer, Berlin.
4. ------ and B. Koren (1986). *A Non-linear Multigrid Method for the Steady Euler Equations.* Proceedings GAMM-Workshop on the Numerical Simulation of Compressible Euler Flows, Rocquencourt 1986, Vieweg, Braunschweig.
5. ------ and S.P. Spekreijse (1986). *Multiple Grid and Osher's Scheme for the Efficient Solution of the Steady Euler Equations.* Appl. Num. Math. 2, 475-493.
6. B. Koren (1988). *Euler Flow Solutions for a Transonic Wind Tunnel Section.* Proceedings High Speed Aerodynamics II, Aachen 1987 (to appear).
7. ------ (1988). *Defect Correction and Multigrid for an Efficient and Accurate Computation of Airfoil Flows.* J. Comput. Phys. (to appear).
8. ------ (1988). *First-Order Upwind Schemes and Multigrid for the Steady Navier-Stokes Equations.* CWI report NM-R88xx (to appear).
9. ------ (1988). *Higher-Order Upwind Schemes and Defect Correction for the Steady Navier-Stokes Equations.* CWI report NM-R88yy (to appear).
10. ------ (1988). *Upwind Schemes for the Navier-Stokes Equations.* Proceedings Second International Conference on Hyperbolic Problems, Aachen, 1988 (to appear).
11. ------ and S.P. Spekreijse (1988). *Solution of the Steady Euler Equations by a Multigrid Method.* Proceedings Third Copper Mountain Conference on Multigrid Methods, Copper Mountain, 1987 (to appear).
12. B. van Leer (1982). *Flux-Vector Splitting for the Euler Equations.* Proceedings 8th International Conference on Numerical Methods in Fluid Dynamics, Aachen 1982, Springer, Berlin.
13. ------ (1985). *Upwind-Difference Methods for Aerodynamic Problems governed by the Euler Equations.* Proceedings 15th AMS - SIAM Summer Seminar on Applied Mathematics, Scripps Institution of Oceanography 1983, AMS, Providence, Rhode Island.
14. S. Osher and F. Solomon (1982). *Upwind-Difference Schemes for Hyperbolic Systems of Conservation Laws.* Math. Comp. 38, 339-374.
15. R. Peyret and T.D. Taylor (1983). *Computational Methods for Fluid Flow.* Springer, Berlin.
16. H. Schlichting (1979). *Boundary-Layer Theory.* McGraw-Hill, New York.
17. S.P. Spekreijse (1987). *Multigrid Solution of Monotone Second-Order Discretizations of Hyperbolic Conservation Laws.* Math. Comp. 49, 135-155.
18. P. Wesseling (1987). *Linear Multigrid Methods.* In: Multigrid Methods, SIAM, Philadelphia.